IEEE Access
Multidisciplinary | Rapid Review | Open Access Journal

Received December 19, 2018, accepted January 5, 2019, date of publication January 9, 2019, date of current version February 8, 2019.

Digital Object Identifier 10.1109/ACCESS.2019.2891663

Time-Energy Optimal Trajectory Planning for Variable Stiffness Actuated Robot

CHEN JI, MINXIU KONG, (Member, IEEE), AND RUIFENG LI, (Member, IEEE)
Key Laboratory of Robotics and Systems, Harbin Institute of Technology, Harbin 150006, China

Corresponding author: Minxiu Kong (jichen1126@163.com)

This work was supported by the National Key R&D Program of China under Grant 2017YFB1303900.

ABSTRACT A variable stiffness actuator is inspired by the human motor control and is the most popular actuator used to exploit the human performance and human-like motion. However, these actuators are typically highly non-linear and redundant not only in their kinematics but also in their dynamics due to their capability to modulate their stiffness and positions simultaneously. It is not trivial to generate the trajectory for a strongly non-linear and redundant dynamic system equipped with variable stiffness actuators. In this paper, a trajectory planning method for a variable stiffness actuated robot via a time-energy optimal control policy is proposed. The simulation studies demonstrate the effectiveness of the trajectory planning method through the case studies of a two degree of freedom variable stiffness actuated robot. Furthermore, the results show that the proposed method could be able to generate the motion which is similar to the human arm motion strategy.

INDEX TERMS Optimal control method, redundant robot, variable stiffness actuator.

I. INTRODUCTION

In the area of robotics, research on human-like motion and human-like performance has been paid great attention to in the last several decades. The trend is changing from merely mutating the biological structure of humans, such as the human arm or an artificial muscle, to researching about the essence of human motions [1], such as the motor control of human muscles [2]. Inspired by the principles of human motor control, a set of biomimetic actuation called variable stiffness actuator has been concentrated on [3] and [4]. The basic idea behind the variable stiffness actuator is to modulate robot stiffness through a mechanical structure instead of a software-based control method [5], such as impedance control or admittance control. The mechanism of variable stiffness actuation can improve performances, like explosive movements [6], [7], safe physical human-robot interaction and adaption to the environment [8]. However, the variable stiffness actuator introduces more complex mechanical structures and hence increases the strong non-linearity to the plant dynamic. What's more, to implement the simultaneous modulation of output position and stiffness of variable stiffness actuators, redundant motors are employed to drive the robot joint. For the above reasons, it is not trivial to deal with this redundancy in motion planning of variable actuated robot [9].

The motion planning of a robot can be divided into two steps [10]. The first step is called trajectory planning. In this step the reference trajectories of actuator motors are generated under kinematic and dynamic constrains. The second step, called trajectory tracking, is to find a control law to track the predefined reference trajectories precisely under model uncertainty and environment disturbance. For variable stiffness actuated robot, the trajectory tracking problem has been paid a lot of attention to in the past decades. Since it is difficult to measure stiffness directly to feedback it into stiffness control loop, the actuator stiffness is compromisingly controlled through position controller as well as actuator position. Based on the Spong's model of compliant actuator, plenty of position controllers, such as singular perturbation-based approaches [11], decoupling-based approaches [12], [13], backstepping-based schemes [14], the Gain scheduling approaches [15], neural network-based approaches [16] and adaptive fuzzy scheme [17], have been designed to deal with the position tracking problem present in variable stiffness actuated robot. However, the study of trajectory planning for variable stiffness actuated robot is still ongoing. Furthermore, considering a task specific scenario, like a ping-pong playing task [18], a gymnastics-like task [19], a ball-throwing task [6] or a

hand-shake task, it is the absence of priori knowledge about how to modulate the stiffness to achieve target performance of these tasks. Obviously, monitoring the arm stiffness variation performance of the human arm while executing a predefined task is one straight and exprimental way to obtain the control law of stiffness. Some scholars employ the optimal control method in order to make use of the intrinsic compliance of variable stiffness actuator [6], [8], [20]. The trajectory planning problem of variable stiffness actuated robot is formulated as an optimal control problem under kinematic and dynamic constrains in a ball-throwing task [21] and a balance control task [22]. In this paper, we study the trajectory planning problem of variable stiffness actuated robot for the reaching point motion task which is very common in human regular life, like catching a ball or putting a cup on the desk. Then the trajectory planning problem of variable stiffness actuated robot is formulated as a time-energy optimal control problem while execution time and energy cost of motion task is treated as performance criterion. In the literature, the time-energy optimal control problem has been reported a lot. The time-optimal trajectory planning of industrial manipulator was firstly presented in [23]. Following this work, the energy cost term was added in the object function of the time-optimal control problem to achieve time-optimal trajectory with reasonable energy cost. To improve the computation efficiency, the problem can be reformulated as the convex form [24]. These previous work are similarly focused on the non-redundantly and rigidly actuated robot with predefined geometric path. Therefore, in case of variable stiffness actuated robot, the previous optimal control methods are not suitable for the strongly non-linearity and redundancy.

To solve the non-linear constrained optimal control problem, there are plenty of candidate optimization methods that can be selected. These methods can be divided into direct method, indirect method and dynamic programming method. In the indirect approach, based on Pontryagin's maximum principle, one attempts to find a solution that satisfies the first-order optimality conditions to the original constrained functional minimization [9], [25]. These conditions are then represented with a two point boundary value problem (TPBVP) which is numerically solved either by using the single shooting method or the multiple shooting method. This method is usually used to analyze the complex optimal control problems, however it is suffered from bad control and state initialization and non-differentiable plant dynamics. In the direct methods, one employs control and/or state parametrization to transform the original optimal control problem to a nonlinear programming problem (NLP). Instead of finding a solution for the first-order optimality conditions, the original infinite dimensional constrained functional minimization is directly converted to a finite dimensional function minimization that is much easier to solve numerically. Indeed, such a function minimization can be solved by using sophisticated NLP methods [10], [24]. However, non-convex objects and constraints function make the optimization computation inefficient and hence converging to a local optimal solution. The attractiveness of the Dynamic programming method is its global-optimal solution compared to the other methods. But instead of using global-optimal solutions derived from Bellman's dynamic programming or variational calculus, there is one branch of dynamic programming called successive approximation methods that only finds sub-optimal solutions and can be iteratively solved to improve the nominal control law efficiently, like the differential dynamic programming (DDP) [26], or the iterative linear quadratic regulator (iLQR) approach [2]. These approaches can help solve the sub-optimal problem on-line which can then be applied in the real time controller design.In this paper, we propose a time-energy optimal control method based on iLQR approach to solve the constrained trajectory generation problem. Firstly, the original time-energy optimal trajectory planning problem with constraints is formulated in section III. Then to handle the inequality constrains for efficient computation, the inequality constrains were normalized and embedded into the system dynamics through transformation of the state space in section IV. Afterward, the proposed method which combines the binary search method of execution time and iLQR approach is presented in detail. To the best of the authors' knowledge, the proposed method has never been reported in the case of variable stiffness actuated robot. To verify the effectiveness of the proposed method, different point-to-point motion tasks on 2-DOF variable stiffness actuated robot have been conducted in section V. Furthermore, the simulation results on serial elastic actuated robot and torque-controlled robot with rigid actuator with same method have been presented to compare with the results of variable stiffness actuated robot to show the influence of the variation stiffness on the execution time and energy cost of motion. The main contribution of this work is a practical optimal control method and the implementation to improve the numerical efficiency for trajectory planning of variable stiffness actuated robot. And it allows scholars to exploit the human-like performance and human-like motion of variable stiffness actuated robot.

The remainder parts of this paper are as follows. The reduced model of variable stiffness actuated robot is recalling in section II and two suggestions are made for the mechanical design. In addition, a roller-cam based mechanism of variable stiffness actuator is presented in section V. Then the case studies of a two-link robot equipped with the roller-cam based variable stiffness actuator is conducted to verify the effectiveness of the proposed method.

II. DYNAMIC MODEL OF VARIABLE STIFFNESS ACTUATED ROBOT

A. GENERAL DYNAMIC MODEL OF ROBOT WITH COMPLIANT JOINTS

The general dynamic model of rigid robot with compliant joints is presented here. Without loss of generality, the flexibility of the robot joints can be introduced by the SEA (Serial Elastic Actuator), VSA (Variable Stiffness

Actuator) or flexible transmission elements. Consider a robot with compliant joints as an open kinematic chain having N + 1 rigid links, which is interconnected by N joints, and actuated by M electrical motors (or hydraulic elements). The link-side coordinates $\boldsymbol{q} \in \mathbb{R}^N$ describes the joint angles and the motor-side coordinates $\boldsymbol{\theta} \in \mathbb{R}^M$ denotes the electric motor angles which is reflected through a gear reduction. Then the kinetic energy, gravitational potential energy and elastic potential energy are defined using the same formalism in [27]. Using the Lagrangian approach, the equation of motion is derived and represented as follows.

$$\begin{bmatrix} \boldsymbol{M}(\boldsymbol{q}) & \boldsymbol{S}(\boldsymbol{q}) \\ \boldsymbol{S}^T(\boldsymbol{q}) & \boldsymbol{J_M} \end{bmatrix} \begin{bmatrix} \ddot{\boldsymbol{q}} \\ \ddot{\boldsymbol{\theta}} \end{bmatrix} + \begin{bmatrix} \boldsymbol{C}(\boldsymbol{q}, \dot{\boldsymbol{q}}, \boldsymbol{\theta}) & \boldsymbol{C}_q(\boldsymbol{q}, \dot{\boldsymbol{q}}) \\ \boldsymbol{C}_\theta(\boldsymbol{q}, \dot{\boldsymbol{q}}) & 0 \end{bmatrix} \begin{bmatrix} \dot{\boldsymbol{q}} \\ \dot{\boldsymbol{\theta}} \end{bmatrix} + \begin{bmatrix} \boldsymbol{D}_q \dot{\boldsymbol{q}} \\ \boldsymbol{D}_\theta \dot{\boldsymbol{\theta}} \end{bmatrix} + \begin{bmatrix} \boldsymbol{G}(\boldsymbol{q}) \\ 0 \end{bmatrix} = \begin{bmatrix} \boldsymbol{\tau}_{E1}(\boldsymbol{q}, \boldsymbol{\theta}) \\ \boldsymbol{\tau}_{E2}(\boldsymbol{q}, \boldsymbol{\theta}) \end{bmatrix} + \begin{bmatrix} 0 \\ \boldsymbol{\tau}_M \end{bmatrix} \quad (1)$$

where $\boldsymbol{M}(\boldsymbol{q}) \in \mathbb{R}^{N \times N}$ is the symmetric and positive definite inertia matrix of the rigid body dynamics,$\boldsymbol{S}(\boldsymbol{q}) \in \mathbb{R}^{N \times M}$ represents the inertial coupling between the rigid body and the motor dynamics, while $\boldsymbol{J_M} \in \mathbb{R}^{M \times M}$ represents the inertia of the motors/gearboxes which is a constant and diagonal matrix. Where $\boldsymbol{C}(\boldsymbol{q}, \dot{\boldsymbol{q}}, \boldsymbol{\theta}) \in \mathbb{R}^{N \times N}$,$\boldsymbol{C}_\theta(\boldsymbol{q}, \dot{\boldsymbol{q}}) \in \mathbb{R}^{M \times M}$, $\boldsymbol{C}_q(\boldsymbol{q}, \dot{\boldsymbol{q}}) \in \mathbb{R}^{N \times M}$ are matrices that represent the Coriolis and normal inertial forces, $\boldsymbol{D}_\theta \dot{\boldsymbol{\theta}} \in \mathbb{R}^M$ and $\boldsymbol{D}_q \dot{\boldsymbol{q}} \in \mathbb{R}^N$ represents the forces due to viscous friction, $\boldsymbol{G}(\boldsymbol{q}) \in \mathbb{R}^N$ is the gravitational force influenced only by the configuration of the robot. $\boldsymbol{\tau}_{E1}(\boldsymbol{q}, \boldsymbol{\theta}) \in \mathbb{R}^N$ are the elastic joint torques that affect the rigid body dynamics and $\boldsymbol{\tau}_{E2}(\boldsymbol{q}, \boldsymbol{\theta}) \in \mathbb{R}^N$ contains the elastic reaction torques that affects the motor dynamics. $\boldsymbol{\tau}_M \in \mathbb{R}^M$ is the motor output torques. Accordingly, the first term in (1) represents the link-side dynamics, while the second term corresponds to the motor-side dynamics. Obviously, the link-side dynamics and the motor-side dynamics influence each other through the elastic torque and inertia coupling.

1) REDUCED DYNAMIC MODEL

Equation (1) is the general form of a robot with compliant joints. The link and motor are not only dynamically coupled through the elastic torque, but also through the inertial coupling components. Considering the influence of these coupling terms makes controlling design difficult, the influence of motor inertia and friction in the system plant should be kept as low as possible at the mechanical design stage. In this paper, one assumption is made to simplify the dynamic model.

A1: the inertia coupling between the rigid body and motor dynamics can be negligible.

Under (A1), the inertial coupling term $\boldsymbol{S}(\boldsymbol{q})$, $\boldsymbol{C}_\theta$, $\boldsymbol{C}_q$ can be eliminated. Then equation (1) can be reduced to

$$\begin{bmatrix} \boldsymbol{M}(\boldsymbol{q}) & 0 \\ 0 & \boldsymbol{J_M} \end{bmatrix} \begin{bmatrix} \ddot{\boldsymbol{q}} \\ \ddot{\boldsymbol{\theta}} \end{bmatrix} + \begin{bmatrix} \boldsymbol{C}(\boldsymbol{q}, \dot{\boldsymbol{q}}, \boldsymbol{\theta}) & 0 \\ 0 & 0 \end{bmatrix} \begin{bmatrix} \dot{\boldsymbol{q}} \\ \dot{\boldsymbol{\theta}} \end{bmatrix} + \begin{bmatrix} \boldsymbol{D}_q \dot{\boldsymbol{q}} \\ \boldsymbol{D}_\theta \dot{\boldsymbol{\theta}} \end{bmatrix} + \begin{bmatrix} \boldsymbol{G}(\boldsymbol{q}) \\ 0 \end{bmatrix} = \begin{bmatrix} \boldsymbol{\tau}_{E1}(\boldsymbol{q}, \boldsymbol{\theta}) \\ \boldsymbol{\tau}_{E2}(\boldsymbol{q}, \boldsymbol{\theta}) \end{bmatrix} + \begin{bmatrix} 0 \\ \boldsymbol{\tau}_M \end{bmatrix} \quad (2)$$

B. VARIABLE STIFFNESS ACTUATOR

The general form of elastic torque which affects the link-side dynamic is represented as

$$\boldsymbol{\tau}_{E1} = \boldsymbol{rF} \quad (3)$$

where $\boldsymbol{r} \in \mathbb{R}^{N \times p}$ is the position matrix of the moment arm and $\boldsymbol{F} \in \mathbb{R}^p$ are the corresponding forces due to the elastic elements (normally the spring is used as elastic element). The torque of common compliant joints is $\boldsymbol{\tau}_{E1}(\boldsymbol{q}, \boldsymbol{\theta}) = \boldsymbol{K}(\boldsymbol{q} - \boldsymbol{\theta})$ in which the moment arm and the joint torsional stiffness $\mathbf{K}$ is a constant matrix [27]. There are two different ways to implement variation of actuator stiffness. One way is the variation of the spring preload. The larger the spring preload, the stiffer the actuator performance [4], this denotes that elastic forces $\boldsymbol{F}$ in (3) can be modulated through motor command angles. The other one is a variation of the transmission ratio between the output and input torques. For instance, according to the lever principle, the output torque is changed along the distance of pivot from the input torque [15], which denotes that the moment arm is adjustable. Combining these two different methods, the elastic torque can be rewritten as.

$$\boldsymbol{\tau}_{E1}(\boldsymbol{q}, \boldsymbol{\theta}) = \boldsymbol{r}(\boldsymbol{\theta})\boldsymbol{F}(\boldsymbol{q}, \boldsymbol{\theta}) \quad (4)$$

1) MOTOR DYNAMIC MODEL

Normally without the direct measurement of stiffness, the stiffness of variable stiffness actuator is compromisingly modulated through the servomotor. Here we introduce the control law and the motor dynamics with the classic high-gain position controller. Under the standard assumption, for the servomotors, of a high transmission ratio and/or of high-gain feedback position controllers, the motor-side dynamics can be considered as decoupled from the link side [27]. As above, if the reduced motor dynamic model is $\boldsymbol{J_M}\ddot{\boldsymbol{\theta}} + \boldsymbol{D}_\theta \dot{\boldsymbol{\theta}} = \boldsymbol{\tau}_{E2}(\boldsymbol{q}, \boldsymbol{\theta}) + \boldsymbol{\tau}_M$, then the classical second-order position controller can be designed as $\boldsymbol{\tau}_M = \hat{\boldsymbol{\tau}}(\boldsymbol{q}, \boldsymbol{\theta}) - \boldsymbol{\xi}\dot{\boldsymbol{\theta}} - \boldsymbol{\kappa}(\boldsymbol{\theta} - \boldsymbol{\theta_d})$ and $\hat{\boldsymbol{\tau}} = -\hat{\boldsymbol{\tau}}_{E2}(\boldsymbol{q}, \boldsymbol{\theta}) + \hat{\boldsymbol{D}}_\theta \dot{\boldsymbol{\theta}}$ is the estimated elastic torque affected by the motor-side dynamics and it is estimated with nominal model parameters. In practice, there always exists model differences between the nominal model and real-world model. The model difference can be handled as a disturbance in the system plant. Furthermore, there are plenty of methods to deal with these disturbance, like disturbance observer. However, this kind of method will not be presented here as it's out of the scope of this paper. Thus the closed-loop dynamics of each servomotors can be represented by a typical second-order linear system which is decoupled as follows.

$$\ddot{\boldsymbol{\theta}} + \boldsymbol{\xi}\dot{\boldsymbol{\theta}} + \boldsymbol{\kappa}\boldsymbol{\theta} = \boldsymbol{\kappa}\boldsymbol{\theta}_d \quad (5)$$

where $\boldsymbol{\theta}_d \in \mathbb{R}^M$ is the reference position of motors for the control loop. $\boldsymbol{\xi} = \mathrm{diag}\{2\alpha_i\} \in \mathbb{R}^{M \times M}$, $\boldsymbol{\kappa} = \mathrm{diag}\{\alpha_i^2\} \in \mathbb{R}^{M \times M}$ are user defined gains as critically damped controller. Since the critically damped controller leads to a fast response without overshooting, this state will not exceed the control input.

III. OPTIMAL CONTROL PROBLEM FORMULATION

In this section, the original time-energy optimal trajectory planning problem with actuation constraints and system dynamic constraints is formulated in detail.

A. PERFORMANCE CRITERION

The general cost function can be represented as

$$J = \Phi(\boldsymbol{x}, \boldsymbol{u}, T) + \int_0^T L(\boldsymbol{x}, \boldsymbol{u}, t)dt \tag{6}$$

where $\Phi(\boldsymbol{x}, \boldsymbol{u}, T) \in \mathbb{R}$ denotes the terminal cost function and $L(\boldsymbol{x}, \boldsymbol{u}, t) \in \mathbb{R}$ denotes the intermediate cost function, while T is defined as the execution time. Then the time-energy optimal object function can be expressed as

$$J = T + \int_0^T \boldsymbol{\tau}_{E1}^{\mathrm{T}} \boldsymbol{\omega}_{energy} \boldsymbol{\tau}_{E1} dt \tag{7}$$

where $\boldsymbol{\tau}_{E1}$ is the output torque of variable stiffness actuator and $\boldsymbol{\omega}_{energy} \in \mathbb{R}^{N\times N}$ is user defined constant matrix which are the weight factor of energy. It is noteworthy that the integral of the square of the elastic torque cannot calculate the energy but it can totally represent the magnitude of the energy consumption [24], [28], [29].

B. SYSTEM DYNAMIC

In this paper, we propose a state-space representation of a variable stiffness actuated robot system that includes the rigid body dynamics of the robot (1) and the closed-loop dynamics of the motors (5). In particular, the control inputs vector is defined as

$$\boldsymbol{u} = \boldsymbol{\theta}_d \in \mathbb{U} \tag{8}$$

where the admission set of control vector is defined as $\mathbb{U} = \{\boldsymbol{u} \in \mathbb{R}^M : \boldsymbol{\theta}_{\min} \leq \boldsymbol{\theta}_d \leq \boldsymbol{\theta}_{\max}\}$, $\boldsymbol{\theta}_{\min}$ and $\boldsymbol{\theta}_{\max}$ are the lower and upper bounds of motor command angles. While the state vector is defined as

$$\boldsymbol{x} = [\boldsymbol{x}_1, \boldsymbol{x}_2, \boldsymbol{x}_3, \boldsymbol{x}_4]^{\mathrm{T}} = [\boldsymbol{q}, \dot{\boldsymbol{q}}, \boldsymbol{\theta}, \dot{\boldsymbol{\theta}}]^{\mathrm{T}} \tag{9}$$

where $\boldsymbol{x} \in \mathbb{R}^{2(M+N)}$ and the initial state is defined as $\boldsymbol{x}_{init}$ and the target state is defined as $\boldsymbol{x}_{target}$. Combining the link-dynamic in equation (2) and motor dynamic in equation (5), the state-space dynamic can be represented as

$$\begin{aligned}\dot{\boldsymbol{x}} &= \boldsymbol{f}(\boldsymbol{x}, \boldsymbol{u}, t) \\ &= \begin{bmatrix} \boldsymbol{x}_2 \\ \boldsymbol{M}(\boldsymbol{x}_1)^{-1}(\boldsymbol{\tau}_{E1}(\boldsymbol{x}_1, \boldsymbol{x}_3) - \boldsymbol{C}(\boldsymbol{x}_1, \boldsymbol{x}_2) \\ \qquad -\boldsymbol{D}(\boldsymbol{x}_2) - \boldsymbol{G}(\boldsymbol{x}_1)) \\ \boldsymbol{x}_4 \\ -\boldsymbol{\xi}\boldsymbol{x}_4 - \boldsymbol{\kappa}\boldsymbol{x}_3 + \boldsymbol{\kappa}\boldsymbol{u} \end{bmatrix}\end{aligned} \tag{10}$$

C. ACTUATION CONSTRAINTS

Regardless of whether the system is compliantly actuated or not, the motor trajectories are subject to inequality constraints due to the range, rate, and acceleration limits posed by their servo controlled dynamics. The admissible set of trajectories subject to these constraints can be defined by

$$\begin{cases} \boldsymbol{\theta}_{\min} \leq \boldsymbol{\theta} \leq \boldsymbol{\theta}_{\max} \\ \dot{\boldsymbol{\theta}}_{\min} \leq \dot{\boldsymbol{\theta}} \leq \dot{\boldsymbol{\theta}}_{\max} \\ \ddot{\boldsymbol{\theta}}_{\min} \leq \ddot{\boldsymbol{\theta}} \leq \ddot{\boldsymbol{\theta}}_{\max} \end{cases} \tag{11}$$

where $\dot{\boldsymbol{\theta}}_{\min}$ and $\dot{\boldsymbol{\theta}}_{\max}$ are the lower and upper bounds of motors angular velocity. $\ddot{\boldsymbol{\theta}}_{\min}$ and $\ddot{\boldsymbol{\theta}}_{\max}$ are the lower and upper bounds of motor acceleration. In addition, due to the physical limits on the deformation of the elastic elements, like the spring deformation, nonlinear state inequality constraints of variable stiffness actuators are satisfied as follows

$$\boldsymbol{\varphi}_{\min} \leq \boldsymbol{\varphi}(\boldsymbol{q}, \boldsymbol{\theta}) \leq \boldsymbol{\varphi}_{\max} \tag{12}$$

where $\boldsymbol{\varphi}(\boldsymbol{q}, \boldsymbol{\theta}) \in \mathbb{R}^{\mathrm{M}}$ is defined as deformation of virtual torsional spring related with joint angles and motor positions. And $\boldsymbol{\varphi}_{\min}$ and $\boldsymbol{\varphi}_{\max}$ are the lower and upper bounds of deformation of the virtual spring respectively. Therefore, the admissible set of state vector subject to these inequality of actuation constraints can be represented as follows.

$$\mathbb{H} = \left\{ \boldsymbol{x} \in \mathbb{R}^{2(M+N)} : \begin{cases} \boldsymbol{\theta}_{\min} \leq \boldsymbol{\theta} \leq \boldsymbol{\theta}_{\max} \\ \dot{\boldsymbol{\theta}}_{\min} \leq \dot{\boldsymbol{\theta}} \leq \dot{\boldsymbol{\theta}}_{\max} \\ \ddot{\boldsymbol{\theta}}_{\min} \leq \ddot{\boldsymbol{\theta}} \leq \ddot{\boldsymbol{\theta}}_{\max} \\ \boldsymbol{\varphi}_{\min} \leq \boldsymbol{\varphi}(\boldsymbol{q}, \boldsymbol{\theta}) \leq \boldsymbol{\varphi}_{\max} \end{cases} \right\} \tag{13}$$

D. OPTIMAL CONTROL PROBLEM

In summary, the original time-energy optimal trajectory planning problem of variable stiffness actuated robot can be expressed as

$$\begin{aligned} \min_{T,u}\ & J = T + \int_0^T \boldsymbol{\tau}_{E1}^{\mathrm{T}} \boldsymbol{\omega}_{energy} \boldsymbol{\tau}_{E1} dt \\ s.t.\ & \dot{\boldsymbol{x}} = \boldsymbol{f}(\boldsymbol{x}, \boldsymbol{u}, t), \\ & \boldsymbol{x}(0) = \boldsymbol{x}_{init}, \\ & \boldsymbol{x}(T) = \boldsymbol{x}_{target}, \\ & \boldsymbol{x} \in \mathbb{H}, \\ & \boldsymbol{u} \in \mathbb{U}. \end{aligned} \tag{14}$$

IV. PROBLEM REFORMULATION BASED ON ILQR APPROACH

To solve the optimal control problem (14) with non-linear plant dynamics, non-linear cost and inequality constraints, the iterative linear quadratic regulator (iLQR) framework is employed in this paper. To improve computation efficiency, a local (quadratic or linear) approximation of the system dynamics and (quadratic approximation) the objective function are used to convert the original optimization problem to a sub-optimal problem [2]. Typically, under the iLQR/DDP frameworks, there are two solutions to handle these constraints. One way is to reconstruct the object function containing the constraints as penalty terms [30]. The other way is to deal with the procedure itself either by solving the sub-optimal problem with state [31] or by controlling constraints [32]. However, under the iLQR framework, solving

an optimal control problem with state inequality constraints and equality constraints is often computationally demanding and complicates the numerical treatment. Therefore, a reduction in the number and complexity of the constraints is often preferred in practice. In the next section, the reformulation of the iLQR approach is presented and a time-energy optimal trajectory planning method to solve the original problem is proposed in (14).

A. HANDLING THE INEQUALITY CONSTRAINTS

To handle the inequality constraints presented above, it is common to treat them as penalty terms and added into the object function which is known as soft constraints. However, particularly, in the case of variable stiffness actuated robot, the violation of the deformation constraints in (12) would not only lead to unexpected results during execution of the planned trajectory, but it would also permanently damage the actuators. Accordingly, it is a priority that the deformation constraints enforced should be strictly satisfied for the real-world application. To achieve this, we present a state space transformation that enables us to explicitly embed the inequality constraints as hard constraints (i.e., constraints that cannot be violated) into the dynamics.

As stated above, the variable stiffness actuated robot is redundantly driven by electrical motors. These motors can be named as position motor and stiffness motor which are in charge of the position modulation and for output stiffness modulation of robot link respectively. Therefore, the original state is defined as

$$\boldsymbol{\theta} = [\boldsymbol{\theta}_{pos}, \boldsymbol{\theta}_{stiff}] \tag{15}$$

where $\boldsymbol{\theta}_{pos} \in \mathbb{R}^N$ are the motor angles for position motor and $\boldsymbol{\theta}_{stiff} \in \mathbb{R}^{M-N}$, M − N are the motor angles of stiffness motor and numbers of these motors, respectively.

The key attribute of variable stiffness actuator is its adjustable compliance. Therefore, it is reasonable that to transform the original state space $[\boldsymbol{q}, \dot{\boldsymbol{q}}, \boldsymbol{\theta}, \dot{\boldsymbol{\theta}}]$ to the new state space $[\boldsymbol{q}, \dot{\boldsymbol{q}}, \boldsymbol{\sigma}, \dot{\boldsymbol{\sigma}}]$. $\boldsymbol{\sigma}$ is defined as

$$\boldsymbol{\sigma} = [\boldsymbol{\sigma}_1, \boldsymbol{\sigma}_2] = [\boldsymbol{\theta}_{stiff}, \boldsymbol{\varphi}(\boldsymbol{q}, \boldsymbol{\theta})] \tag{16}$$

Without loss of generality, the inequality constraints about the new system states $\boldsymbol{\sigma}$ are defined as a general form:

$$\Delta = \{\boldsymbol{\sigma}^{[i]}_{\min} \le \boldsymbol{\sigma}^{[i]} \le \boldsymbol{\sigma}^{[i]}_{\max}, \quad i = 1, \ldots, M\} \tag{17}$$

To embed these constraints into the dynamics, we may proceed in the following transformation with the uniform expression being rewritten as

$$\Delta = \{\bar{\boldsymbol{\sigma}} \in [0, 1] : \bar{\boldsymbol{\sigma}}^{[i]} = \frac{\boldsymbol{\sigma}^{[i]} - \boldsymbol{\sigma}^{[i]}_{\min}}{\boldsymbol{\sigma}^{[i]}_{\max} - \boldsymbol{\sigma}^{[i]}_{\min}}, \quad i = 1, \ldots, M\} \tag{18}$$

Therefore, the admissible set of control vector and state vectors are redefined as

$$\mathbb{U} = \{\bar{\boldsymbol{\sigma}}_d \in \mathbb{R}^M : 0 \le \bar{\boldsymbol{\sigma}}_d \le 1\} \tag{19}$$

$$\bar{\boldsymbol{x}} = [\bar{\boldsymbol{x}}_1, \bar{\boldsymbol{x}}_2, \bar{\boldsymbol{x}}_3, \bar{\boldsymbol{x}}_4]^{\mathrm{T}} = [\boldsymbol{q}, \dot{\boldsymbol{q}}, \bar{\boldsymbol{\sigma}}, \dot{\bar{\boldsymbol{\sigma}}}]^{\mathrm{T}} \tag{20}$$

However, the task of how to embed the new state variables into the dynamics is still a challenge remaining to be solved. Considering the transformation in (18), the relationship among $\boldsymbol{\sigma}$, $\boldsymbol{\theta}$ and $\boldsymbol{q}$ can expressed with an implicit function as below

$$\boldsymbol{\Psi}^{[i]}(\boldsymbol{q}, \boldsymbol{\theta}, \boldsymbol{\sigma}) = 0 \tag{21}$$

where $\boldsymbol{\Psi}^{[i]}(\boldsymbol{q}, \boldsymbol{\theta}, \boldsymbol{\sigma}) \triangleq \boldsymbol{\sigma}^{[i]} - \boldsymbol{\sigma}^{[i]}_{\min} - \left(\boldsymbol{\sigma}^{[i]}_{\max} - \boldsymbol{\sigma}^{[i]}_{\min}\right) \bar{\boldsymbol{\sigma}}^{[i]}$, $i = 1, \ldots, M$. It is noteworthy that the proposed transformation favors constraints which lead to an analytical form for explicitly representing the original state. Therefore, according to the implicit function theorem [33], if the given function $\boldsymbol{\Psi}$ is continuously differentiable then the determinant of its Jacobian matrix as nonzero is as follows.

$$\det[\partial \boldsymbol{\Psi} / \partial \boldsymbol{\theta}] \ne 0 \tag{22}$$

Thus the original state vector $\boldsymbol{\theta}$ for every $(\boldsymbol{q}, \boldsymbol{\sigma})$ can be obtained uniquely through

$$\boldsymbol{\theta} = \boldsymbol{\Psi}^{-1}(\boldsymbol{q}, \boldsymbol{\sigma}) \tag{23}$$

Through the transformation of the state vector, the inequality constraints about angles of stiffness adjusting motor $\boldsymbol{\theta}_{stiff}$ and deformations $\boldsymbol{\varphi}(\boldsymbol{q}, \boldsymbol{\theta})$ are eliminated and embedded into the system dynamics, which means that under the control threshold in (19) the state inequality constraint of deformation in (12) and stiffness motor position in (11) will not be violated. However, except these embedded constraints, there are other constraints that cannot be embedded into the system dynamics. To deal with these constraints, (23) is substituted to (11), and the new constraints are transformed through derivatives with respect to time and can be rewritten as

$$\begin{cases} \boldsymbol{\theta}_{\min} \le \boldsymbol{\Psi}^{-1}(\boldsymbol{q}, \boldsymbol{\sigma}) \le \boldsymbol{\theta}_{\max} \\ \dot{\boldsymbol{\theta}}_{\min} \le d\boldsymbol{\Psi}^{-1}(\boldsymbol{q}, \boldsymbol{\sigma})/dt \le \dot{\boldsymbol{\theta}}_{\max} \\ \ddot{\boldsymbol{\theta}}_{\min} \le d^2\boldsymbol{\Psi}^{-1}(\boldsymbol{q}, \boldsymbol{\sigma})/dt^2 \le \ddot{\boldsymbol{\theta}}_{\max} \end{cases} \tag{24}$$

Therefore, the aforementioned constraints are transformed to constraints related with the new system state. According to the augmented Lagrange method, these constraints are treated as soft constraint (constructed as penalty terms and added into the intermediate cost function in (7)). Furthermore, the final state equality constraint in (14) for reaching the target point, a quadratic cost function is introduced and added to the terminal cost function in (7).

B. SYSTEM DYNAMIC TRANSFORMATION

Substituting the new system state (20), (23) and control variables (19), the new state-space dynamic can be represented as

$$\dot{\bar{\boldsymbol{x}}} = \bar{\boldsymbol{f}}(\bar{\boldsymbol{x}}, \bar{\boldsymbol{\sigma}}_d, t) = \begin{bmatrix} \bar{\boldsymbol{x}}_2 \\ \boldsymbol{M}(\bar{\boldsymbol{x}}_1)^{-1}(\boldsymbol{\tau}_{E1}(\bar{\boldsymbol{x}}_1, \boldsymbol{\Psi}^{-1}(\bar{\boldsymbol{x}}_1, \bar{\boldsymbol{x}}_3)) \\ \quad -\boldsymbol{C}(\bar{\boldsymbol{x}}_1, \bar{\boldsymbol{x}}_2) - \boldsymbol{D}(\bar{\boldsymbol{x}}_2) - \boldsymbol{G}(\bar{\boldsymbol{x}}_1)) \\ \bar{\boldsymbol{x}}_4 \\ -\boldsymbol{\xi}\bar{\boldsymbol{x}}_4 - \boldsymbol{\kappa}\bar{\boldsymbol{x}}_3 + \boldsymbol{\kappa}\bar{\boldsymbol{\sigma}}_d \end{bmatrix} \tag{25}$$

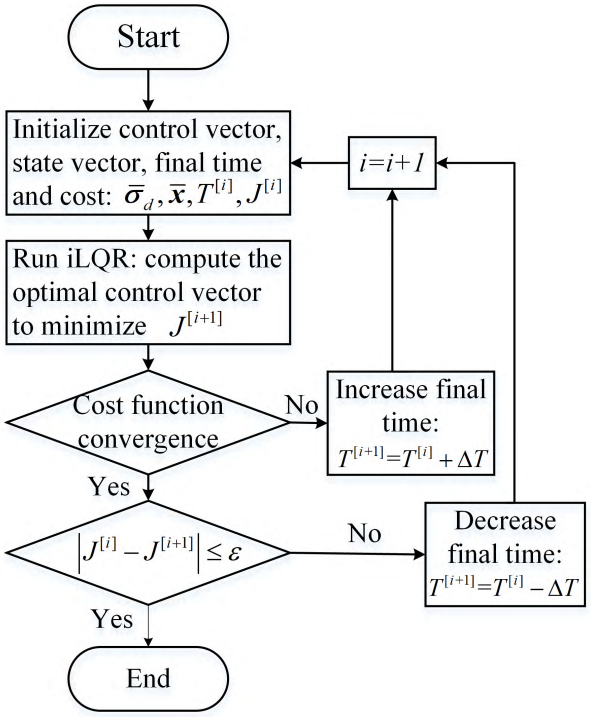

FIGURE 1. Time-energy optimal method based on iLQR.

C. TIME-ENERGY OPTIMAL TRAJECTORY PLANNING PROBLEM

As mentioned above, the original time-energy optimal trajectory planning problem is reformulated through the transformation of state space and embedded into the inequality constraints into the system dynamics. Thus the reformulated optimal control problem can be rewritten as follows.

$$\begin{aligned}\min_{T,u}\ & J = \omega_{target}\|\bar{\boldsymbol{x}}(T)-\bar{\boldsymbol{x}}_{target}\|^2 + T \\ & \quad + \int_0^T \left(\boldsymbol{\tau}_{E1}^{\mathrm{T}}\boldsymbol{\omega}_{energy}\boldsymbol{\tau}_{E1}\right) dt + \omega_{rate}\sum_{i=0}^{N_c}\|P(g_i)\|^2 \\ s.t.\ & \dot{\bar{\boldsymbol{x}}} = \bar{\boldsymbol{f}}(\bar{\boldsymbol{x}}, \bar{\boldsymbol{\sigma}}_d, t), \\ & \bar{\boldsymbol{x}}(0) = \bar{\boldsymbol{x}}_{init}, \\ & \bar{\boldsymbol{\sigma}}_d \in \mathbb{U}. \end{aligned} \tag{26}$$

where ω_{target}, $\boldsymbol{\omega}_{energy}$, ω_{rate} are the weight factors of consumed energy, speed and acceleration of motors, respectively. $\|*\|^2$ is the Euclidean norm operator. N_c is the constraints number. $\omega_{target}\|\bar{\boldsymbol{x}}(T)-\bar{\boldsymbol{x}}_{target}\|^2$ is the quadratic cost function which is introduced as a terminal term into the cost function. $g_i(\bar{\boldsymbol{x}})$ represents the inequality or equality constraints in (24). $P(g)$ denotes the penalty function of constraints which can be defined based on either the exterior or the interior method [34]. In this case, because it is easier to find the initial guess of a feasible point rather than an infeasible one, the logarithmic barrier function $log(g_i)$ is employed to reconstruct these constraints as penalty terms. What's more, the inequality constraints should be satisfied and $g_i(\bar{\boldsymbol{x}}) \ge 0$.

Algorithm 1 iLQR(iterative Linear Quadratic Regulator)

```
procedure ilqr
    Initialize the state and control sequence in step1.
    repeat
        K, k ← BackwardPass
        x*σ*_d, δJ ← ForwardPass K, k
    until |δJ| ≤ 1e^-6
end procedure
function BackwardPass
    for i = N to 0 do
        Compute the derivatives of f, J with x, u.
        Compute the cost-to-go function Q_i;
        Optimal control gains K^[i], k^[i] ← arg min Q_i.
    end for
end function
function ForwardPass(x, u, K, k)
    repeat
        α = 1
        for i = 0 to N do
            σ_d^[i+1] ← σ_d^[i] + αk^[i] + K^[i]δx
            x^[i+1] ← f(x^[i], u^[i])
        end for
        α ← decrease line-search update rule
        δJ ← J_old − J_new;
    until δJ ≤ 0
end function
```

1) PROPOSED SOLUTION METHOD

The proposed method to solve the time-energy optimal control problem is illustrated in Fig.1 and the process in detail is presented as follows:

Step1: Initialize the control vector $\bar{\boldsymbol{\sigma}}_d$ and state vector $\bar{\boldsymbol{x}}$ with a given maximum final time $T^{[i]}$. Then the initial cost $J^{[i]}$ can be computed. The grid of control and state variables are defined as N.

Step2: The iLQR frameworks is employed to solve the time-energy problem (26) and the optimal control vector and minimization of cost function $J^{[i+1]}$ are obtained. The procedure of iLQR is presented in Algorithm 1 and more detail can be found in [2].

Step3: If the optimal control problem was not converging to the given small threshold, the final time was to be increased by $\Delta T = 0.5\left(T^{[i]} - T_{\min}\right)$ and the new lower bounds of final time to be updated as $T_{\min} = T^{[i]}$. Then step1 and step2 are to be repeated.

Step4: If the optimal control problem can obtain the convergence results and additionally the new optimal cost value should be satisfied $|J^{[i]} - J^{[i+1]}| \le \varepsilon$, which means to judge whether the last optimal cost value is closer enough with the new one, then the optimization process will be exited. ε is the user defined threshold. If the condition is not satisfied, then final time of motion is to be decreased with $\Delta T = 0.5\left(T^{[i]} - T_{\min}\right)$ and step1 and step2 to be repeated.

Through the proposed method, the optimal control $\bar{\boldsymbol{\sigma}}_d^*$ and optimal state vector $\bar{\boldsymbol{x}}^*$ are obtained. However, the

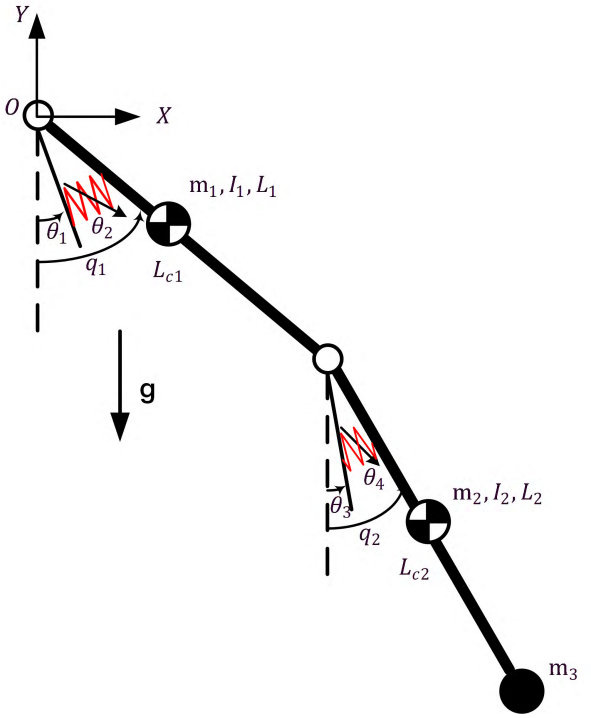

FIGURE 2. Schematic drawing of two-link variable stiffness actuated robot with prototype of stiffness variation at each actuator. The physical parameters of dynamics are reported in the next section.

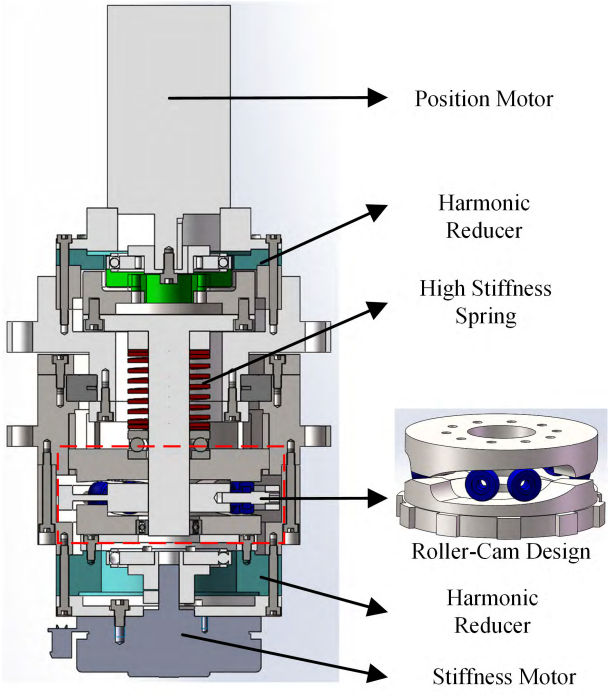

FIGURE 3. Mechanical design of variable stiffness actuator based on roller-cam mechanism. Three pairs of roller are connected to the output link and driven by position motor. One cam disk is fixed to link side and the second to stiffness motor. The cam disks are axially pushed together by the high stiffness spring and are rotationally supported by multiple spline (not shown).

optimal trajectory of position motors and stiffness motors are implicitly expressed by $\bar{\sigma}$. There exists the following relationship $\Psi^{[i]}(q, \theta, \sigma) \triangleq \sigma^{[i]} - \sigma^{[i]}_{\min} - \left(\sigma^{[i]}_{\max} - \sigma^{[i]}_{\min}\right)\bar{\sigma}^{[i]}, i = 1, \ldots, M$. According to the implicit function theorem, the original state vector θ can be obtained through $\theta = \Psi^{-1}(q, \sigma)$. Therefore, the optimal θ^* are obtained.

V. CASE STUDY OF 2-DOF VARIABLE STIFFNESS ACTUATED ROBOT

In this section, a model of 2-DOF variable stiffness actuated robot in Fig.2 is built to verify the proposed method for the time-energy optimal trajectory planning problem. Based on roller-cam design [4] for stiffness modulation depicted in Fig.3, a new design of variable stiffness actuator is introduced and the stress analysis of cam-roller design is presented in Fig.4. In particular, the output elastic torque of actuator is derived briefly. Afterward, the actuation constraints of the proposed actuator and the modeling of link-side dynamics are introduced in detail. To verify the proposed method in the last section, different cases with four target locations are defined to be solved. Furthermore, the same optimal control problem of serial elastic actuated robot and torque-controlled rigid robot are compared with the variable stiffness actuated robot.

A. MODEL OF 2-DOF VARIABLE STIFFNESS ACTUATED ROBOT

1) ACTUATION CONSTRAINS

As shown in the Fig.3, the introduced variable stiffness actuator contains a position motor, harmonic reducer, stiffness

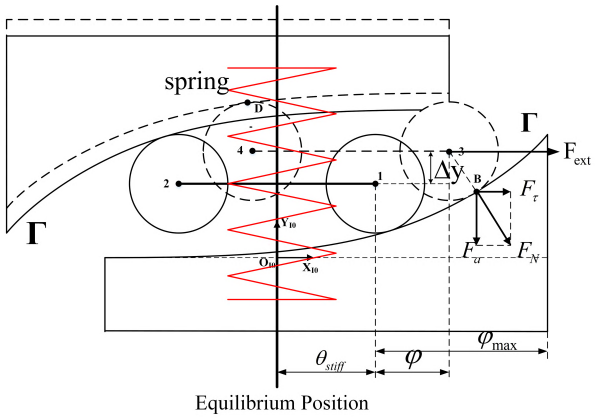

FIGURE 4. Schematic view and stress analysis for roller-cam mechanism. The equilibrium position depends on the stiffness layout position θ_{stiff}. And when applying the external torque F_{ext} on the link, the roller will deviate from the equilibrium position and the cam disks will axially push the spring and generate the spring force. The tangential force F_τ applied on the cam disk moment arm is the output elastic torque and the centripetal force F_α counterbalances the spring force.

motor and a roller-cam design based stiffness modulation mechanism. The Roller-cam mechanism is the core of variable stiffness actuator. It has two opposed cam disks and three pairs of rollers which are embraced by cam disks. The out shaft of position motor is connected with the roller by harmonic reducer. Its rotation will lead to the rotation of

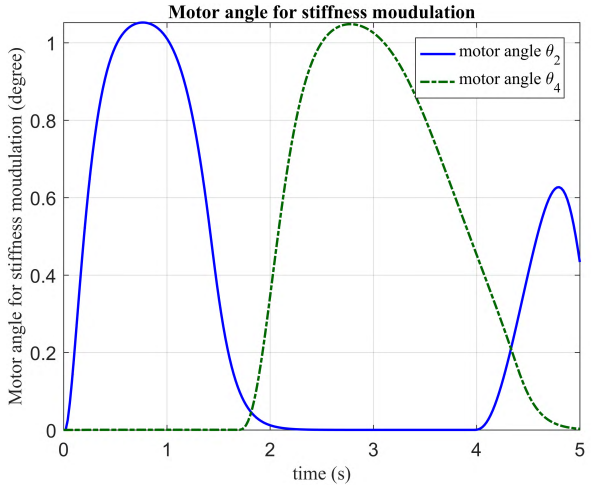

(a)

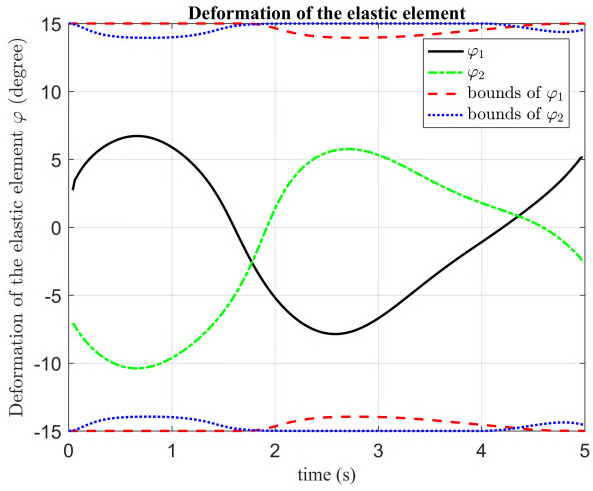

(b)

FIGURE 5. The motor trajectories of stiffness modulation in CASE1. In figure (b), the blue Dotted lines and the red Dashed lines are the lower and upper bounds define in (29) while is not violated during the entire point to point motion. (a) Motor angles for the stiffness modulation. (b) The deformation of the roller-cam mechanism.

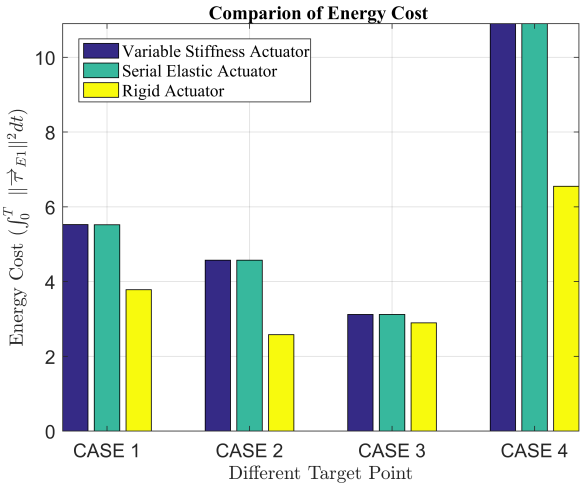

(a)

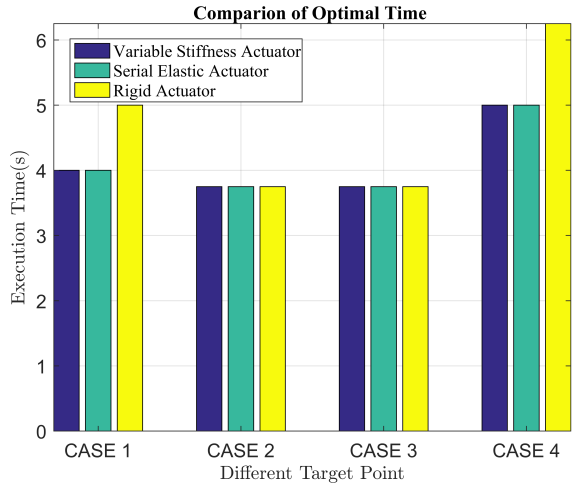

(b)

FIGURE 6. Optimal energy cost and execution time comparison between variable stiffness actuated robot, serial elastic actuated robot and torque controlled stiff actuated robot. (a) Optimal energy cost comparison. (b) Optimal execution time comparison.

robot link. The two cam disks are pushed together through a high stiffness spring. If there is relative rotation between roller and cam disks, the deformation of spring will produce the axial spring force which will lead to the output torque through the moment arm. Regarding the variation in stiffness, the relative angular position of the two cam disks can be changed by the stiffness motor. And due to the nonlinearity of cam curve depicted in Fig.4, the closer the two cam disks are, the higher the initial output stiffness. Therefore, the output initial stiffness can be changed by adjusting the stiffness motor.

Through the static stress analysis for roller-cam mechanism in Fig. 4, the elastic torque can be expressed as follows.

$$\boldsymbol{\tau}_{E1} = \mathrm{K} \cdot \Delta y \cdot \mathrm{R}_{cam} \left(\frac{\partial \Gamma}{\partial \boldsymbol{\varphi}}(\boldsymbol{\varphi}) - \frac{\partial \Gamma}{\partial \boldsymbol{\varphi}}(-\boldsymbol{\varphi}) \right) \tag{27}$$

where K is spring stiffness and Δy is defined as a compression of the spring. The deformation of virtual torsional spring is defined as $\boldsymbol{\varphi} \in \{\mathbb{R}^2 : \varphi_i = q_i - \theta_{i+2}, i = 1, 2\}$. The cam disk profile is designed as an exponential curve and is defined as $\Gamma = e^{\rho_{char}(\boldsymbol{\varphi} - \boldsymbol{\theta}_{stiff})}$, ρ_{char} is characteristic constant of the designed cam disk profile, $\boldsymbol{\theta}_{stiff} = [\theta_2, \theta_4] \in \mathbb{R}^2$ represents the stiffness setup angles. R_{cam} is a constant which represents the moment arm. Substituting the cam disk profile Γ into the equation (27), the output elastic torques are reformulated as follows.

$$\boldsymbol{\tau}_{E1} = \boldsymbol{\tau}_{\max} e^{\rho_{char}(-\boldsymbol{\varphi}_{\max} + \boldsymbol{\theta}_{stiff})} \left(e^{\rho_{char}\boldsymbol{\varphi}} - e^{-\rho_{char}\boldsymbol{\varphi}} \right) \tag{28}$$

where $\boldsymbol{\tau}_{E1} = [\tau_1, \tau_2] \in \mathbb{R}^2$. $\boldsymbol{\tau}_{\max} \in \mathbb{R}^2$ is a user-defined maximum output torque vector when the maximum deformation of spring is achieved. As shown in Fig.4, the deformation of the virtual spring is limited by the length of the cam disk curve. And the maximum of the deformation is influenced

TABLE 1. Four case with different target states.

Case Number	Link-side angle(rad)	Link-side angle velocity(rad/s)
CASE 1	$[1.57, 0]$	$[0, 0]$
CASE 2	$[0, 0]$	$[0, 0]$
CASE 3	$[0, 1.57]$	$[0, 0]$
CASE 4	$[1.57, 1.57]$	$[0, 0]$

TABLE 2. Simulation parameters.

Symbol	Parameter	Value/Unit
ω_{target}	weight factor of target tracking	400
$\boldsymbol{\omega}_{energy}$	weight factor of energy cost	$\begin{bmatrix} 0.01 & 0 \\ 0 & 0.01 \end{bmatrix}$
ω_{rate}	weight factor of motor velocity and acceleration	0.01
$\boldsymbol{\varphi}_{\max}$	maximum deformation of elastic element	0.2617rad
$\boldsymbol{\kappa}$	stiffness coefficient in motor position controller	$\begin{bmatrix} 250 & 0 & 0 & 0 \\ 0 & 250 & 0 & 0 \\ 0 & 0 & 100 & 0 \\ 0 & 0 & 0 & 100 \end{bmatrix}$ N/m
$\boldsymbol{\xi}$	damping coefficient in motor position controller	$\begin{bmatrix} 50 & 0 & 0 & 0 \\ 0 & 50 & 0 & 0 \\ 0 & 0 & 10 & 0 \\ 0 & 0 & 0 & 10 \end{bmatrix}$ N/(m/s)
ρ_{char}	characteristic coefficient of cam disk curve	12
ε	the optimization tolerance	0.5
R	the moment arm of elastic torque	33mm
K	spring stiffness	8000N/m
$T^{[0]}$	initial execution time	5s
$\boldsymbol{\tau}_{\max}$	bounds of the maximum output torque	$[-5, 5]$N · m
$[\boldsymbol{\theta}^{stiff}_{\min}, \boldsymbol{\theta}^{stiff}_{\max}]$	bounds of stiffness motor angle	$[0, 0.174]$rad
$[\dot{\boldsymbol{\theta}}^{stiff}_{\min}, \dot{\boldsymbol{\theta}}^{stiff}_{\max}]$	bounds of stiffness motor velocity	$[-1.96, 1.96]$rad/s
$[\ddot{\boldsymbol{\theta}}^{stiff}_{\min}, \ddot{\boldsymbol{\theta}}^{stiff}_{\max}]$	bounds of stiffness motor acceleration	$[-10, 10]$rad/s
$[B_1, B_2]$	viscous friction coefficient	$[0.01, 0.01]$Nms/rad
$[m_1, m_2]$	mass of link1 and link2	$[0.5, 0.5]$kg
$[I_1, I_2]$	inertia of link1 and link2	$[0.5, 0.5]$kg · m^2
$[L_1, L_2]$	length of link1 and link2	$[0.5, 0.5]$m
$[L_{c1}, L_{c2}]$	the center of mass of link1 and link2	$[0.5, 0.5]$m
$\boldsymbol{x}_{init}$	initial state	$[-1.57, 0, 0, 0, 0, 0, 0, 0, 0, 0, 0, 0]$

by the stiffness setup. The relation between deformation constraints and stiffness setup is shown as follows.

$$-\boldsymbol{\varphi}_{\max} + \boldsymbol{\theta}_{stiff} \leq \boldsymbol{\varphi} \leq \boldsymbol{\varphi}_{\max} - \boldsymbol{\theta}_{stiff} \tag{29}$$

2) SYSTEM DYNAMICS

The vector of link-side angles describing the rotation of the two links is defined as $\boldsymbol{q} = [q_1, q_2]$ and the inertia matrix $\boldsymbol{M}(\boldsymbol{q}) = \begin{pmatrix} m_{11} & m_{12} \\ m_{21} & m_{22} \end{pmatrix}$, the Coriolis and normal inertial terms $\boldsymbol{C}(\boldsymbol{q}, \dot{\boldsymbol{q}}) = [c_1, c_2]$, the viscous friction $\boldsymbol{D}(\dot{\boldsymbol{q}}) = [d_1, d_2]$ and the gravity terms $\boldsymbol{G}(\boldsymbol{q}) = [g_1, g_2]$ are defined as follows.

$$\begin{aligned}
m_{11} &= I_1 + m_1 L_{c1} + I_2 + m_2 \left(L_1^2 + 2L_1 L_{c2} \cos q_2 + L_{c2}^2\right) \\
&\quad + m_3 \left(L_1^2 + 2L_1 L_2 \cos q_2 + L_2^2\right) \\
m_{12} &= m_{21} = I_2 + m_2 \left(L_{c2}^2 + 2L_1 L_{c2} \cos q_2\right) \\
&\quad + m_3 \left(L_2^2 + 2L_1 L_2 \cos q_2\right) \\
m_{22} &= I_2 + m_2 L_{c2}^2 + m_3 L_2^2
\end{aligned}$$

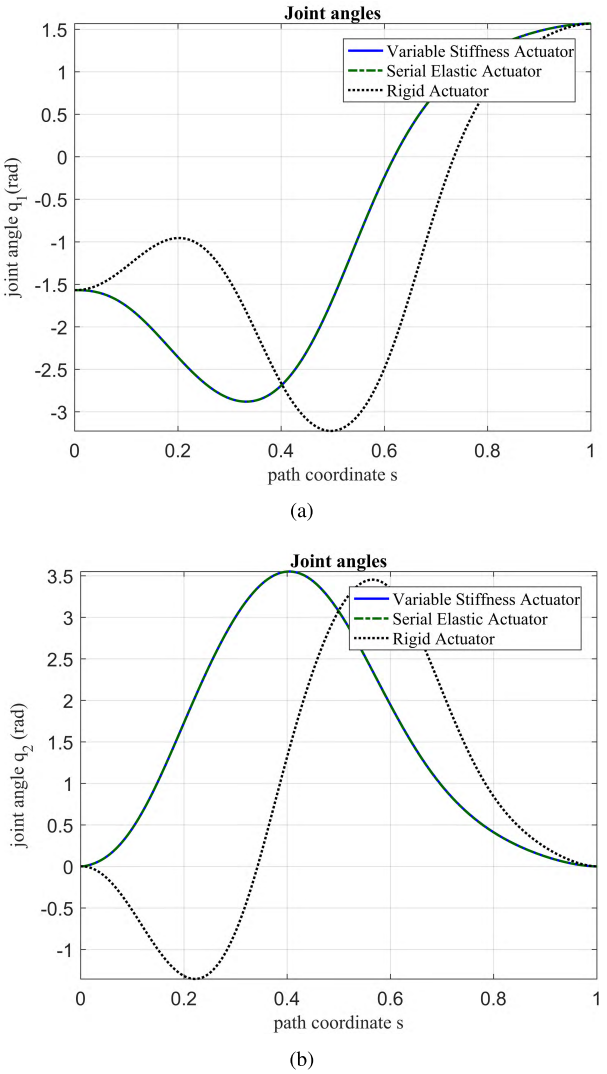

FIGURE 7. The link-side trajectory in CASE 1. For comparison in same time scale, the path parameter $\{s \in \mathbb{R}, 0 \leq s \leq 1\}$ is introduced to scale different execution times into the nominal parameter space. And in the rest of paper, the comparisons among different actuators are also transformed to the parameter space. (a) Joint angle q_1. (b) Joint angle q_2.

$$\begin{aligned}
c_1 &= -\left(m_2 L_{c2} + m_3 L_2\right) L_1 \sin q_2 \left(2\dot{q}_1 \dot{q}_2 + {\dot{q}_2}^2\right) \\
c_2 &= \left(m_2 L_{c2} + m_3 L_2\right) L_1 \sin q_2 \left({\dot{q}_1}^2\right) \\
d_1 &= B_1 \dot{q}_1 \\
d_2 &= B_2 \dot{q}_2 \\
g_1 &= g\left(m_1 L_{c1} + m_2 L - 1 + m_3 L_1\right) \cos q_1 \\
&\quad + g\left(m_2 L_{c2} + m_3 L_2 \cos\left(q_1 + q_2\right)\right) \\
g_2 &= g\left(m_2 L_{c2} + m_3 L_2\right) \cos\left(q_1 + q_2\right)
\end{aligned} \tag{30}$$

where m_i, L_i, L_{ci}, I_i, B_i, $i = 1, 2$ are, respectively, the mass, the length of the i-th link, the center of mass and the moment of inertia of the same link.

B. OPTIMIZATION RESULTS

In this section, to verify the proposed method in the last section, simulations on variable stiffness actuated robot are

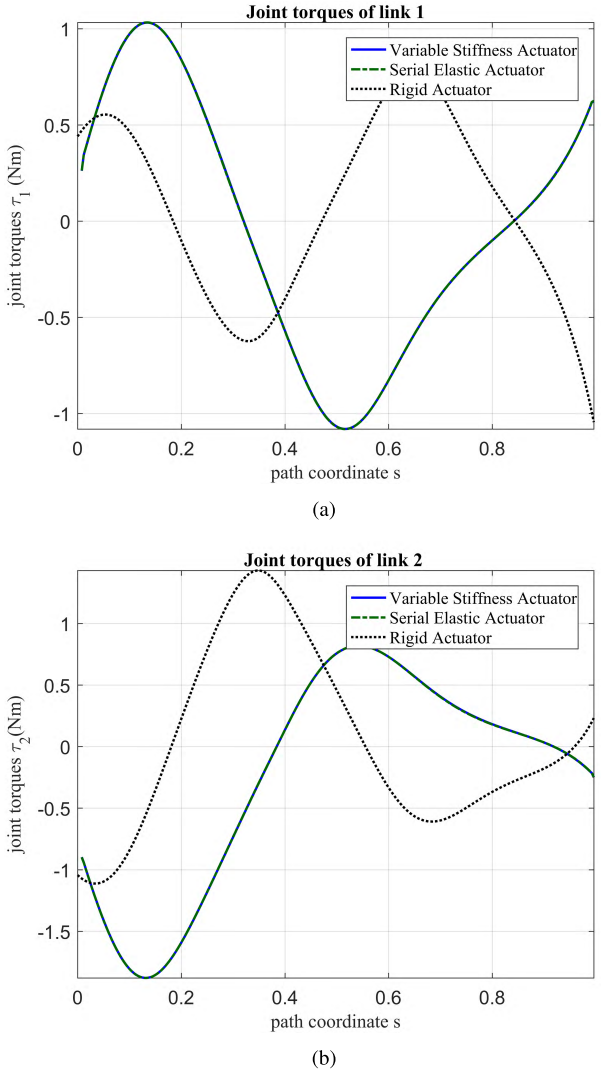

FIGURE 8. The joint torques in CASE 1. (a) Joint torque of link1. (b) Joint torque of link2.

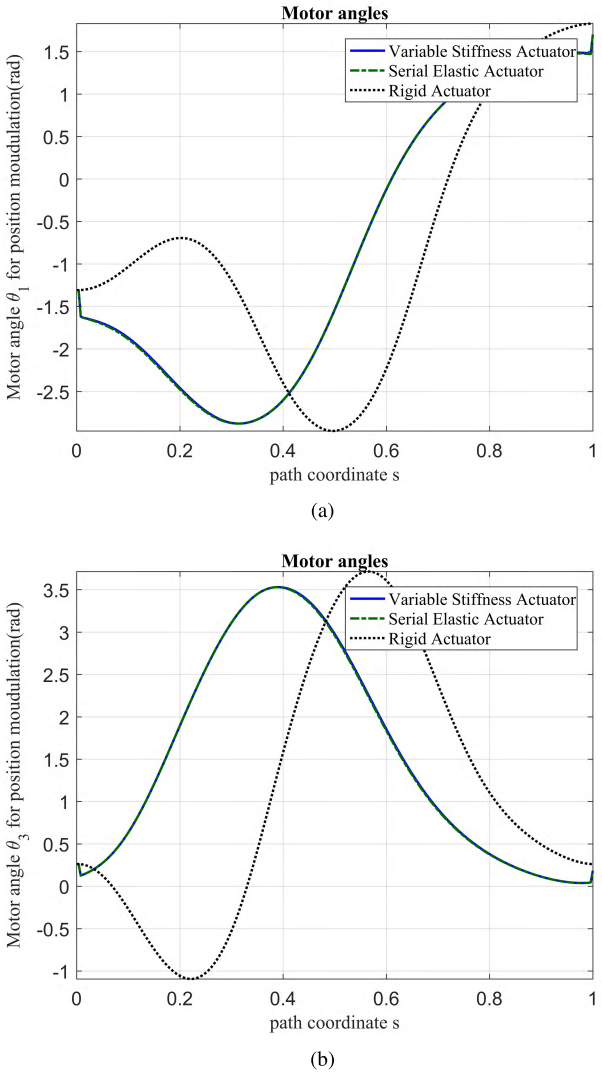

FIGURE 9. The position motor trajectories in CASE 1. (a) Joint angle θ_1. (b) Joint angle θ_2.

carried out in which different point-to-point motion cases with four target locations are defined. Meanwhile, the simulations of same trajectory planning problem on serial elastic actuated robot and torque-controlled rigidly actuated robot are also conducted with the proposed method. Four different target locations are defined as shown in Table1. Furthermore, the necessary parameters used in the simulations are summarized in the Table2. The simulations were conducted in two different ways. One way to solve the time-energy trajectory planning problem is via the proposed method. The four different target locations are able to be achieved successfully through the proposed method in the above section. Concerning the redundancy of variable stiffness actuator, the variation of stiffness was also successfully generated through the proposed optimal control method. The stiffness motor angles in CASE 1 is illustrated in Fig.5. It is found that the stiffness might be modulated to be larger to get through energy cost position during the target reaching task. As shown in Fig.5, at the beginning of the motion which is during 0-2s, the stiffness of the first actuator was stiffened up and during 2-4s of the entire motion the second actuator was stiffened up. In addition, the bounds of the motor angles and deformation are not violated during the motion. Hence it is confirmed that the proposed method is effective for the trajectory planning problem of variable stiffness actuated robot.

The other way is that the proposed method was also applied in the case of robot actuated with serial elastic actuator and torque-controlled rigid actuator. The results of optimal time and energy cost are depicted in Fig.6. As shown in the results, the execution time and energy cost in variable stiffness actuated and serial elastic actuated robot are close to each other. Since in the rigid actuator there is a lack of compliant elements, the energy efficiency is higher than the other ones. The results of joint angles, joint torques and position motor angles of CASE 1 are depicted in Fig.7, Fig.8 and Fig.9 respectively.

Among the three actuators, the motions are all energy-based and while reaching the target location the link will swing back and forth to gain more energy through gravity potential energy instead of directly relying on the input power through servo motors. The interesting difference among the three different actuators is that the second link swings backward first to gain more velocity through gravity potential energy in the case of rigid actuator while in the others the first link swings backward at the beginning. The optimal policy for complaint actuator seems more cautious than the torque controlled rigid actuator and it is similar to the human motion called forearm leads upper arm motion strategy [35], such as ball-throwing or weaving racket in tennis.

VI. CONCLUSION

In this article, we demonstrated the trajectory planning problem of variable stiffness actuated robot. To solve this problem, time-energy optimal control method based on iLQR framework was proposed. Using this method, the complexity of the problem was reduced and the computation efficiency was improved. In addition, a new type of variable stiffness actuator based on roller-cam design was introduced and the stress analysis was presented as well. Considering the simulation results, we found out that the optimal control solution can perform the similar control policy in the human arm motion which is called the forearm leads upper arm motion strategy.

In the future work, we intend to investigate the optimal control method through the experiment on variable stiffness actuated robot platform.

REFERENCES

[1] S. Wolf *et al.*, "Variable stiffness actuators: Review on design and components," *IEEE/ASME Trans. Mechatronics*, vol. 21, no. 5, pp. 2418–2430, Oct. 2016.
[2] E. Todorov and W. Li, "A generalized iterative LQG method for locally-optimal feedback control of constrained nonlinear stochastic systems," in *Proc. Amer. Control Conf.*, vol. 1, Jun. 2005, pp. 300–306.
[3] L. Chen *et al.*, "Optimal control for maximizing velocity of the CompAct compliant actuator," in *Proc. IEEE Int. Conf. Robot. Autom.*, May 2013, pp. 516–522.
[4] S. Wolf, O. Eiberger, and G. Hirzinger, "The DLR FSJ: Energy based design of a variable stiffness joint," in *Proc. IEEE Int. Conf. Robot. Autom.*, May 2011, pp. 5082–5089.
[5] C. Ott, A. Albu-Schäffer, A. Kugi, and G. Hirzinger, "On the passivity-based impedance control of flexible joint robots," *IEEE Trans. Robot.*, vol. 24, no. 2, pp. 416–429, Apr. 2008.
[6] D. Braun, M. Howard, and S. Vijayakumar, "Optimal variable stiffness control: Formulation and application to explosive movement tasks," *Auto. Robots*, vol. 33, no. 3, pp. 237–253, 2012.
[7] M. Garabini, A. Passaglia, F. Belo, P. Salaris, and A. Bicchi, "Optimality principles in stiffness control: The VSA kick," in *Proc. IEEE Int. Conf. Robot. Automat. (ICRA)*, May 2012, pp. 3341–3346.
[8] M. Garabini, A. Passaglia, F. Belo, P. Salaris, and A. Bicchi, "Optimality principles in variable stiffness control: The VSA hammer," in *Proc. IEEE/RSJ Int. Conf. Intell. Robots Syst. (IROS)*, Sep. 2011, pp. 3770–3775.
[9] M. H. Korayem, H. R. Nohooji, and A. Nikoobin, "Path planning of mobile elastic robotic arms by indirect approach of optimal control," *Int. J. Adv. Robotic Syst.*, vol. 8, no. 1, p. 10, 2011.
[10] M.-X. Kong, C. Ji, Z.-S. Chen, and R.-F. Li, "Smooth and near time-optimal trajectory planning of robotic manipulator with smooth constraint based on cubic B-spline," in *Proc. IEEE Int. Conf. Robot. Biomimetics (ROBIO)*, Dec. 2013, pp. 2328–2333.
[11] M. Spong, K. Khorasani, and P. Kokotovic, "An integral manifold approach to the feedback control of flexible joint robots," *IEEE J. Robot. Autom.*, vol. JRA-3, no. 4, pp. 291–300, Aug. 1987.
[12] F. Petit and A. Albu-Schäffer, "State feedback damping control for a multi DOF variable stiffness robot arm," in *Proc. IEEE Int. Conf. Robot. Autom.*, May 2011, pp. 5561–5567.
[13] G. Palli, C. Melchiorri, and A. De Luca, "On the feedback linearization of robots with variable joint stiffness," in *Proc. IEEE Int. Conf. Robot. Autom.*, May 2008, pp. 1753–1759.
[14] F. Petit, A. Daasch, and A. Albu-Schäffer, "Backstepping control of variable stiffness robots," *IEEE Trans. Control Syst. Technol.*, vol. 23, no. 6, pp. 2195–2202, Nov. 2015.
[15] I. Sardellitti, G. A. Medrano-Cerda, N. Tsagarakis, A. Jafari, and D. G. Caldwell, "Gain scheduling control for a class of variable stiffness actuators based on lever mechanisms," *IEEE Trans. Robot.*, vol. 29, no. 3, pp. 791–798, Jun. 2013.
[16] Z. Guo, Y. Pan, T. Sun, Y. Zhang, and X. Xiao, "Adaptive neural network control of serial variable stiffness actuators," *Complexity*, vol. 2017, pp. 1–9, Nov. 2017, Art. no. 5361246.
[17] M. N. Nguyen, D. T. Tran, and K. K. Ahn, "Robust position and vibration control of an electrohydraulic series elastic manipulator against disturbance generated by a variable stiffness actuator," *Mechatronics*, vol. 52, pp. 22–35, Jun. 2018.
[18] O. Koç, G. Maeda, and J. Peters, "Online optimal trajectory generation for robot table tennis," *Robot. Auton. Syst.*, vol. 105, pp. 121–137, Jul. 2018.
[19] J. Nakanishi, A. Radulescu, D. J. Braun, and S. Vijayakumar, "Spatio-temporal stiffness optimization with switching dynamics," *Auto. Robots*, vol. 41, no. 2, pp. 273–291, 2016.
[20] D. J. Braun *et al.*, "Robots driven by compliant actuators: Optimal control under actuation constraints," *IEEE Trans. Robot.*, vol. 29, no. 5, pp. 1085–1101, Oct. 2013.
[21] A. Zhakatayev, M. Rubagotti, and H. A. Varol, "Time-optimal control of variable-stiffness-actuated systems," *IEEE/ASME Trans. Mechatronics*, vol. 22, no. 3, pp. 1247–1258, Jun. 2017.
[22] B. Ugurlu *et al.*, "Variable ankle stiffness improves balance control: Experiments on a bipedal exoskeleton," *IEEE/ASME Trans. Mechatronics*, vol. 21, no. 1, pp. 79–87, Feb. 2016.
[23] J. E. Bobrow, S. Dubowsky, and J. S. Gibson, "Time-optimal control of robotic manipulators along specified paths," *Int. J. Robot. Res.*, vol. 4, no. 3, pp. 3–17, Sep. 1985.
[24] D. Verscheure, B. Demeulenaere, J. Swevers, J. De Schutter, and M. Diehl, "Time-optimal path tracking for robots: A convex optimization approach," *IEEE Trans. Autom. Control*, vol. 54, no. 10, pp. 2318–2327, Oct. 2009.
[25] M. Kong, Z. Chen, C. Ji, W. You, and M. Liu, "Optimal point-to-point motion planning of heavy-duty industry robot with indirect method," in *Proc. IEEE Int. Conf. Robot. Biomimetics (ROBIO)*, Dec. 2013, pp. 768–773.
[26] D. Q. Mayne, *Differential Dynamic Programming—A Unified Approach to the Optimization of Dynamic Systems*, vol. 10. New York, NY, USA: Academic, 1973, pp. 179–254.
[27] B. Siciliano and O. Khatib, *Springer Handbook of Robotics*, vol. 56, no. 8. Berlin, Germany: Springer, 2007, pp. 987–1008.
[28] A. Gasparetto and V. Zanotto, "A technique for time-jerk optimal planning of robot trajectories," *Robot. Comput.-Integr. Manuf.*, vol. 24, no. 3, pp. 415–426, 2008.
[29] Z. Shiller, "Time-energy optimal control of articulated systems with geometric path constraints," *J. Dyn. Syst., Meas., Control*, vol. 118, no. 1, pp. 139–143, 1996.
[30] D. J. W. Ruxton, "Differential dynamic programming applied to continuous optimal control problems with state variable inequality constraints," *Dyn. Control*, vol. 3, no. 2, pp. 175–185, Apr. 1993.
[31] Z. Xie, C. K. Liu, and K. Hauser, "Differential dynamic programming with nonlinear constraints," in *Proc. IEEE Int. Conf. Robot. Automat. (ICRA)*, May 2017, pp. 695–702.
[32] Y. Tassa, N. Mansard, and E. Todorov, "Control-limited differential dynamic programming," in *Proc. IEEE Int. Conf. Robot. Automat. (ICRA)*, May 2014, pp. 1168–1175.
[33] T. M. Apostol, *Mathematical Analysis*. Reading, MA, USA: Addison-Wesley, 1974.
[34] J. Nocedal and J. Stephen Wright, *Interior-Point Methods for Nonlinear Programming*. New York, NY, USA: Springer, 2006, pp. 563–597.
[35] S. Haddadin, F. Huber, and A. Albu-Schäffer, "Optimal control for exploiting the natural dynamics of Variable Stiffness robots," in *Proc. IEEE Int. Conf. Robot. Automat. (ICRA)*, May 2012, pp. 3347–3354.

CHEN JI received the M.S. degree from the Harbin Institute of Technology, Harbin, China, in 2013, where he is currently pursuing the Ph.D. degree with the State Key Laboratory of Robotics and System. His research interests include variable stiffness actuation and optimal control methods.

MINXIU KONG is currently an Assistant Professor with the State Key Laboratory of Robotics and System, School of Mechatronics Engineering, Harbin Institute of Technology, China. His research interests include industrial robots and nonlinear control theory.

RUIFENG LI is currently a Professor and a Ph.D. Candidate Supervisor with the State Key Laboratory of Robotics and System, School of Mechatronics Engineering, Harbin Institute of Technology, China. His research interests include industrial robots and service robots.